Active-Clamped Zero-Current Switching Current-Fed Half-Bridge Converter

Cassiano Ferro Moraes, Emerson Giovani Carati, Jean Patric da Costa, Rafael Cardoso, and Carlos Marcelo de Oliveira Stein

***Abstract*—This article presents an auxiliary circuit for the current-fed half-bridge (CFHB) converter, aiming to clamp the high voltage spikes across the main switches caused by the energy stored in the leakage inductance of the transformer. This circuit also provides zero-current switching (ZCS) to the main switches at turn-OFF. Moreover, the rectifier diodes and the auxiliary switch operates under ZCS at turn-ON and turn-OFF. Another feature of the proposed circuit is that it is composed of just one active switch, reducing the number of auxiliary sources and drivers compared to the conventional active-clamped CFHB converter. In addition, the inclusion of the clamping circuit increases the voltage ratio of the converter. A 300-W prototype was built to validate the analysis and design proposed in this article. The converter was tested for various load conditions at 100 kHz, and a peak efficiency of 96.2% was obtained. Also, a comparison of efficiency for the CFHB employing other conventional clamping circuits is presented.**

***Index Terms*—Converters, dc–dc power conversion, photovoltaic (PV) power systems.**

I. Introduction

GREEN energy systems applied in distributed generation have been a trend in academic and industrial research. Alternative sources for low power applications, such as photovoltaic (PV) microinverters and portable fuel cells have grown significantly. Aiming to interface these low-voltage energy sources with the electrical grid, high step-up dc–dc converters have been adopted in microinverters to provide a voltage level in the dc-bus higher than the peak of line voltage [1]–[4]. To establish a high-voltage ratio without galvanic isolation, some nonisolated topologies have been proposed [5]–[9]. However, a large duty cycle value near one is necessary when coupled inductors or cascaded converters are not used. As a result, higher current and voltage stresses occur, as well as reverse recovery problems in the semiconductors, increasing converter losses and reducing efficiency [9]–[12].

In order to provide a high-voltage ratio with galvanic isolation, dc–dc converters with high-frequency (HF) transformers have been used. These converters can ensure safety as well as reduce noise and electromagnetic interference (EMI) in power transfer, which is significant for grid-tied applications [13]. Among isolated topologies, current- and voltage-fed converters have been widely applied in PV and fuel cell generation [14]–[17]. Compared to voltage-fed, current-fed converters have smaller input current ripple and higher transformer utilization factor, which makes these converter suitable for microinverter applications. Within these topologies, the current-fed half-bridge converter (CFHB) has half the number of active switches compared to the full-bridge topology, having lower implementation cost and volume [1].

Just as other isolated topologies, the CFHB topology suffers from high-voltage spikes and ringing across the switches at turn-OFF, caused by energy stored in the leakage inductance of the transformer. These problems lead to stress and losses in semiconductors and increase EMI [18], [19]. Besides, due to the overvoltages, active switches with higher breakdown voltage levels must be used, which may reduce converter efficiency since the on-resistance is proportional to the drain-source voltage [20].

Passive snubbers and active-clamp circuits have been adopted to absorb the energy stored in the leakage inductance and minimize its effects in isolated converters [21]. Despite reducing overvoltages and generally being simpler to design, passive snubbers usually dissipate energy, decreasing converter efficiency.

To achieve high efficiency and limit voltage spikes, active clamp circuits have been applied to isolated converters in high step-up applications [22]–[24]. These auxiliary circuits may improve converter efficiency by providing soft-switching, thus lower switching losses can be achieved, and the overvoltages across semiconductors are reduced. Therefore, it is possible to increase switching frequency aiming to reduce the size of the converters.

In the literature, some active-clamping circuits have been proposed for the CFHB converter. An active-clamped CFHB (ACCFHB) with a full-wave rectifier was proposed in [25]. The auxiliary circuit is composed of two switches and a capacitor to clamp the voltage across the main switches. One of the advantages of this auxiliary circuit is that zero-voltage

Manuscript received July 25, 2019; revised November 1, 2019; accepted December 3, 2019. Date of publication December 10, 2019; date of current version March 13, 2020. This work was supported in part by the Research and Development Project PD 2866-0468/2017, granted by the Brazilian Electricity Regulatory Agency (ANEEL) and Companhia Paranaense de Energia (COPEL), in part by the Funding Authority for Studies and Projects (FINEP), in part by the Coordination for the Improvement of Higher Level or Education-Personnel (CAPES), in part by the Brazilian National Council for Scientific and Technological Development (CNPq), in part by Fundação Araucária, and in part by the Universidade Tecnológica Federal do Paraná (UTFPR). Recommended for publication by Associate Editor W. Huang. *(Corresponding author: Carlos Marcelo de Oliveira Stein.)*

The authors are with the Universidade Tecnológica Federal do Paraná (UTFPR), Pato Branco 85503-390, Brazil (e-mail: cassianofmoraes@gmail.com; emerson@utfpr.edu.br; jpcosta@utfpr.edu.br; rcardoso@utfpr.edu.br; cmstein@utfpr.edu.br).

Color versions of one or more of the figures in this article are available online at http://ieeexplore.ieee.org.

Digital Object Identifier 10.1109/TPEL.2019.2959447

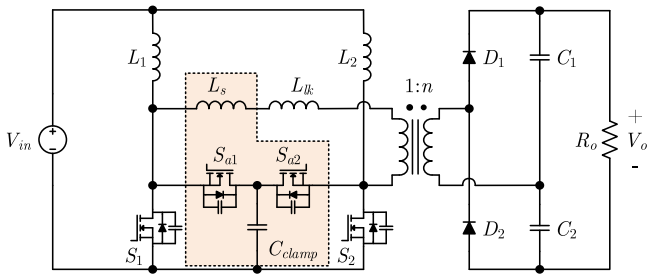

Fig. 1. Conventional ACCFHB converter presented in [28] with voltage doubler rectifier.

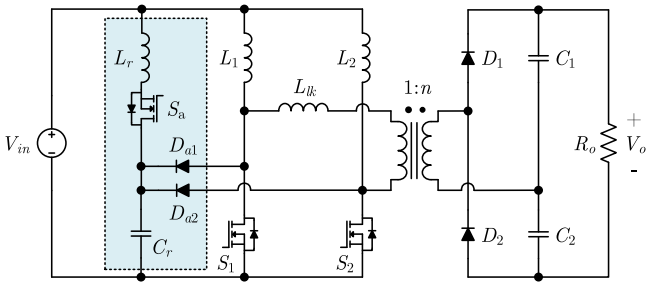

Fig. 2. Proposed ACCFHB converter.

switching (ZVS) is provided for all switches at turn-ON. Nevertheless, it requires two extra drivers to control the clamping circuit, increasing the cost and volume of the converter. The ACCFHB was better analyzed in [26] and [27] for various load and input voltage values to rate the ZVS range. The ACCFHB with the auxiliary circuit connected to the bottom was presented in [28]. This converter employing a voltage doubler rectifier is presented in Fig. 1. In [29], an analysis of two connection types of the clamp capacitor in the ACCFHB was performed to compare the effects on the input current and efficiency.

In this article, an active-clamped zero-current-switching (ZCS) CFHB converter is proposed. The overall circuit diagram is shown in Fig. 2. This clamping circuit was based on [30], with some changes in the connection and design considerations. One of the advantages of the proposed auxiliary circuit is that it absorbs the leakage inductance energy to clamp the voltage spikes and ringing across the main switches. Also, it provides ZCS condition at turn-OFF to these semiconductors and ZCS at turn-ON and turn-OFF for the rectifier diodes. The clamping circuit design considers the internal leakage inductance value, thus it is not necessary to add an external series inductor with the transformer. Moreover, this clamping circuit increases the voltage ratio of the conventional CFHB; therefore, a lower value of duty cycle is needed for the main switches. The auxiliary circuit operates under ZCS condition, thus the switching frequency can be increased, reducing the size of the prototype. With the clamping action in the main and auxiliary circuit, semiconductors with lower breakdown voltage levels may be used, which generally features lower on-resistance, contributing to reduce conduction losses.

This article is organized as follows. In Section II, the detailed operation stages of the proposed converter are described. Section III presents the design considerations of the proposed clamping circuit, and also a basic comparison of the proposed ACCFHB to others presented in the literature. Section IV shows the experimental results of the implemented prototype. In Section V, a power losses analysis is performed to compare the performance of the proposed auxiliary circuit to other clamping circuits. Finally, Section VI concludes this article.

II. Operation Stages Of The Proposed Converter

The proposed converter is composed of two parts: the conventional CFHB converter and the active-clamping circuit, which is highlighted in Fig. 2. The standard CFHB converter with voltage doubler rectifier is composed of input voltage V_{in}, inductors L_1 and L_2, the main switches S_1 and S_2, the rectifier diodes D_1 and D_2, and capacitors C_1 and C_2. The auxiliary circuit is composed of switch S_a, diodes D_{a1} and D_{a2}, clamping capacitor C_r, and resonant inductor L_r.

To simplify the analysis of the proposed converter, it is considered that $L_1 = L_2 = L$ and $C_1 = C_2 = C$. Moreover, the voltages across C_1 and C_2, as well as the current through L_1 and L_2, are considered constant during a switching period. The current through these inductors is determined by

$$I_L \approx \frac{P_o}{2V_{\text{in}}} \tag{1}$$

where P_o is the output power.

The steady-state analysis is described for the eight operation stages that compose one half-cycle of the switching period, considering a complete commutation of S_1. The main waveforms of the converter are shown in Fig. 3, the state planes are presented in Fig. 4, and the operation stages are summarized in Fig. 5.

Stage 1 (t_0, t_1): At t_0, capacitor C_r is charged with a voltage level equal to V_{clamp}. This stage begins when S_a is turned ON. A resonance is established between C_r and L_r, so S_a is naturally turned ON under ZCS condition. At the end of this stage, C_r is clamped with a voltage level equal to zero. The voltage over the clamping capacitor and the current through L_r are determined by the following equations:

$$v_{C_r}(t) = (V_{\text{clamp}} - V_{\text{in}})\cos(\omega_1(t - t_0)) + V_{\text{in}} \tag{2}$$

$$i_{L_r}(t) = \frac{V_{\text{clamp}} - V_{\text{in}}}{Z_1}\sin(\omega_1(t - t_0)) \tag{3}$$

where the angular resonance frequency $\omega_1 = 1/\sqrt{L_r C_r}$ and the characteristic impedance $Z_1 = \sqrt{L_r/C_r}$.

From the state plane shown in Fig. 4(a), the following equation calculates the duration of this stage

$$\Delta t_1 = \frac{1}{\omega_1}\left[\frac{\pi}{2} + \sin^{-1}\left(\frac{V_{\text{in}}}{V_{\text{clamp}} - V_{\text{in}}}\right)\right]. \tag{4}$$

The current through L_r at the end of the first stage is designed to be equal to $2I_L$, thus ZCS condition is provided to the main switches. This condition is established by

$$I_{L_r}(t_1) = \frac{V_{\text{clamp}} - V_{\text{in}}}{Z_1}\sin(\omega_1 \Delta t_1). \tag{5}$$

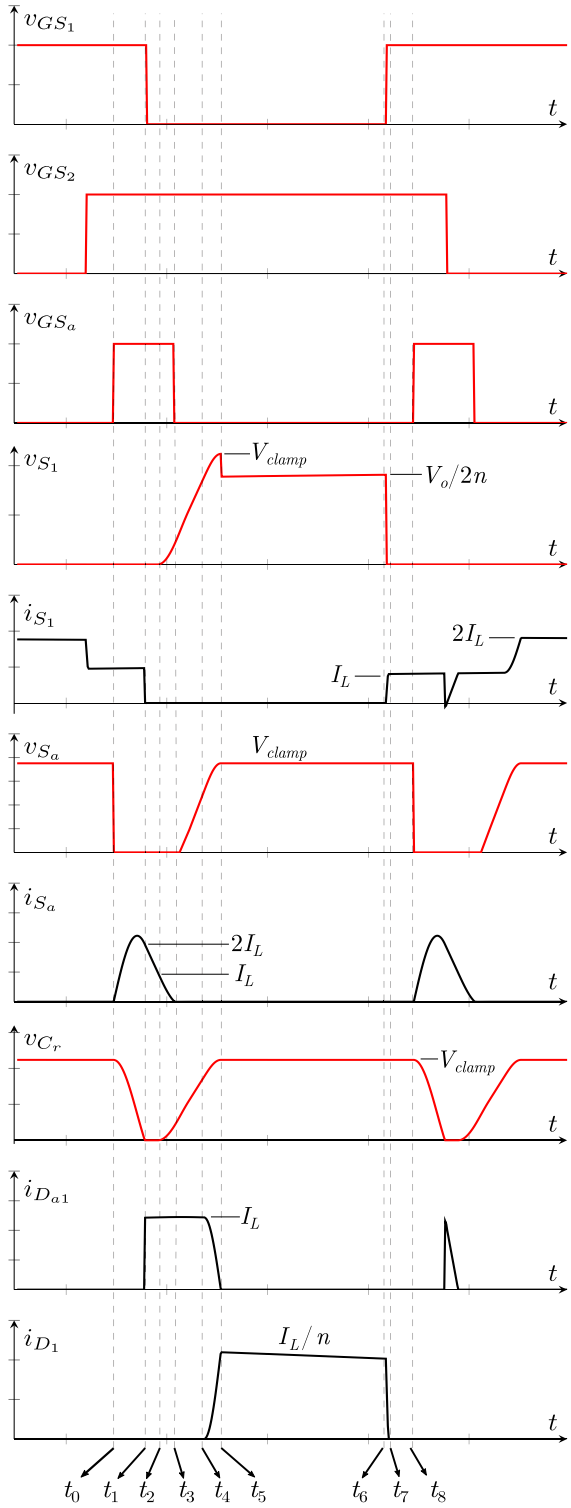

Fig. 3. Main waveforms of the proposed converter for half a switching cycle.

Stage 2 (t_1, t_2): The auxiliary diodes D_{a1} and D_{a2} start conducting a current value equals I_L. The current through L_r decreases from $2I_L$ to I_L and it is defined by

$$i_{L_r}(t) = 2I_L - \frac{V_{\text{in}}}{L_r}(t - t_1). \tag{6}$$

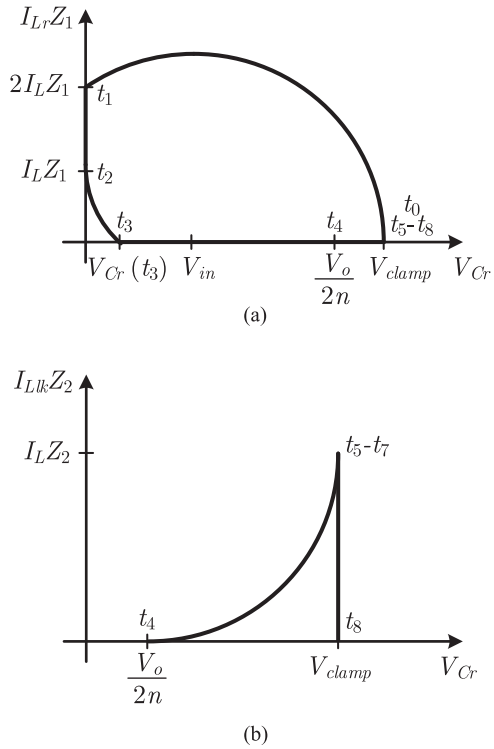

Fig. 4. State plane for the proposed converter. (a) V_{C_r} and I_{Lr}. (b) V_{C_r} and I_{Llk}.

At the end of this stage, the current through D_{a2} decreases from I_L to zero, and the voltage across this semiconductor remains zero. Therefore, this diode turns OFF under ZCS condition.

The following equation determines the duration for the second stage

$$\Delta t_2 = \frac{L_r}{V_{\text{in}}} I_L. \tag{7}$$

Stage 3 (t_2, t_3): A resonance is established between L_r and C_r, and the current through this inductor decreases to zero. Thus, S_a is turned OFF under ZCS. The current through L_r is determined by

$$i_{L_r}(t) = I_L - \frac{V_{\text{in}}}{Z_1} \sin(\omega_1(t - t_2)). \tag{8}$$

The voltage across the clamping capacitor is expressed by the following equation:

$$v_{C_r}(t) = V_{\text{in}} \left[1 - \cos(\omega_1(t - t_2))\right]. \tag{9}$$

The time duration for stage 3 is determined by

$$\Delta t_3 = \frac{1}{\omega_1} \sin^{-1}\left(\frac{I_L Z_1}{V_{\text{in}}}\right). \tag{10}$$

Stage 4 (t_3, t_4): This stage begins when S_a is turned OFF under ZCS condition. C_r is linearly charged by I_L through D_{a1} as follows:

$$v_{C_r}(t) = \frac{I_L}{C_r}(t - t_3). \tag{11}$$

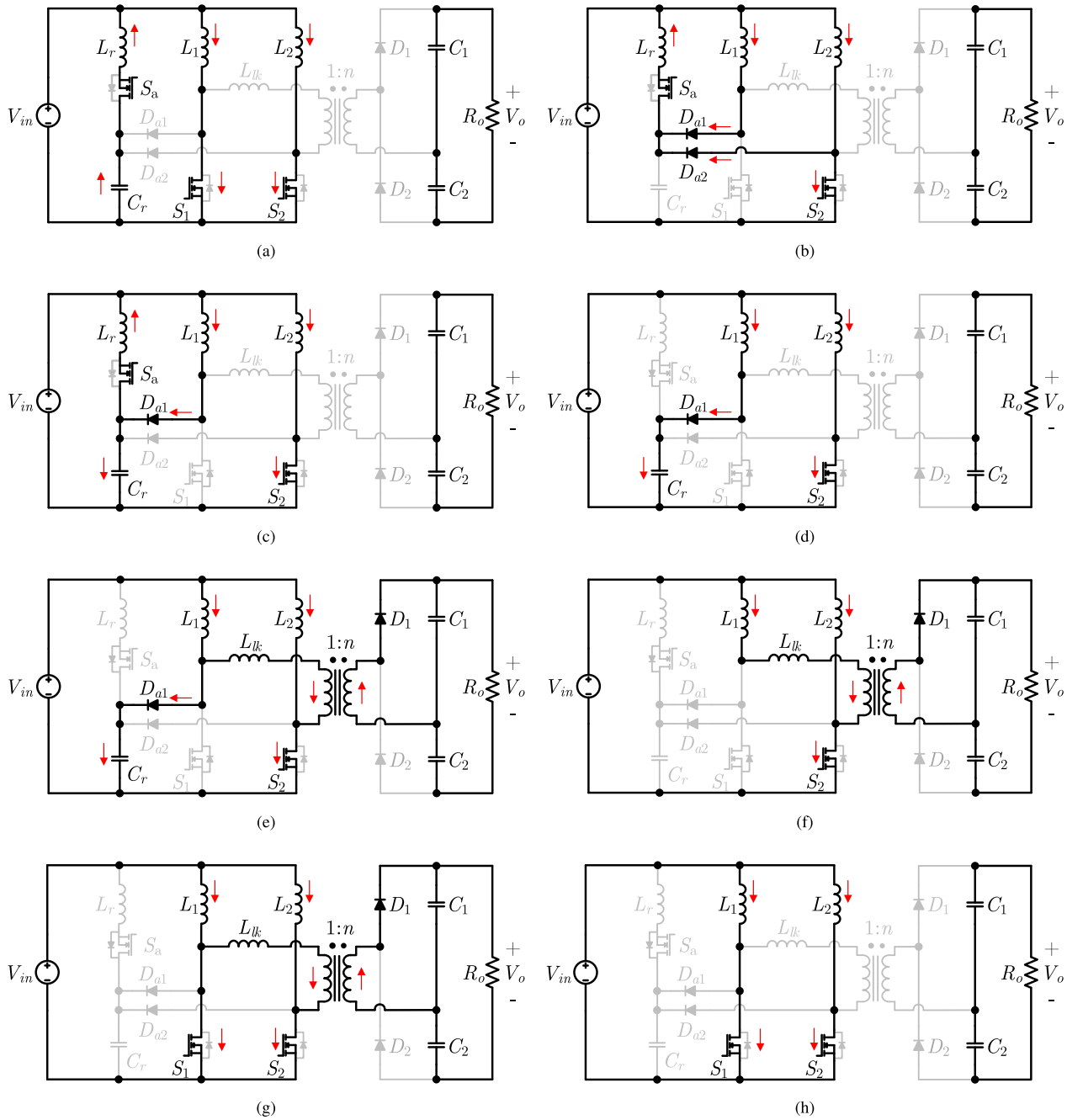

Fig. 5. Operation stages of the proposed converter. (a) Stage 1. (b) Stage 2. (c) Stage 3. (d) Stage 4. (e) Stage 5. (f) Stage 6. (g) Stage 7. (h) Stage 8.

This step ends when the voltage across the clamping capacitor reaches $V_o/(2n)$. The following equation expresses the duration of the fourth stage

$$\Delta t_4 = \left(\frac{V_o}{2n} - V_{Cr}(t_3)\right)\frac{C_r}{I_L}. \tag{12}$$

Stage 5 (t_4, t_5): At the beginning of this stage, the current through D_{a1} starts to decrease, and the transformer is energized. A resonance is established between L_{lk} and C_r, influenced by the primary winding of the HF transformer. Therefore, the voltage across S_1 is expressed as follows:

$$v_{S_1}(t) = v_{C_r}(t) = Z_2 I_L \sin\left(\omega_2(t - t_4)\right) + \frac{V_o}{2n} \tag{13}$$

where angular resonance frequency $\omega_2 = 1/\sqrt{L_{lk}C_r}$ and characteristic impedance $Z_2 = \sqrt{L_{lk}/C_r}$. The following equation determines the clamping voltage across S_1

$$V_{\text{clamp}} = Z_2 I_L + \frac{V_o}{2n}. \tag{14}$$

Owing to the resonance during this step, rectifier diode D_1 turns ON under ZCS. The current through this diode is expressed as follows:

$$i_{D_1}(t) = \frac{i_{L_{lk}}(t)}{n} = \frac{I_L}{n}\Big[1 - \cos(\omega_2(t - t_4))\Big]. \quad (15)$$

From the state plane presented in Fig. 4(b), the duration time of this stage is calculated by (16). At the end of this stage, D_{a1} turns OFF under ZCS, and C_r voltage reaches V_{clamp}. Therefore, the voltage across S_1 gets clamped in this value

$$\Delta t_5 = \frac{\pi}{2\omega_2}. \quad (16)$$

Stage 6 (t_5, t_6): The converter operates as a conventional CFHB converter. The voltage across L_1 and L_2 is equal to V_{in}, and the output capacitors provide energy to the load.

Stage 7 (t_6, t_7): The seventh stage begins when S_1 is turned ON. The current through this switch increases up to I_L, while the current through D_1 decreases to zero, both linearly. Thus, ZCS condition is achieve for this diode. The following equation determines the duration of the seventh operation stage

$$\Delta t_7 = \frac{L_{lk} I_L 2n}{V_o}. \quad (17)$$

Stage 8 (t_7, t_8): In this stage, the converter operates as a conventional CFHB.

III. Analysis And Design Considerations

A. Voltage Conversion Ratio

The voltage ratio of the proposed converter can be determined by imposing the volt-second rule on L_1 or L_2. By analyzing the operation stages, the voltage conversion ratio M can be expressed as

$$M = A - \sqrt{A^2 - B} \quad (18)$$

where

$$A = \frac{2nI_L}{C_r V_{\text{in}} f_s}\left(1 - D - \frac{L_r I_L f_s}{V_{\text{in}}}\right), B = \frac{8n^2 I_L}{C_r V_{\text{in}} f_s}$$

where D is the duty cycle, and f_s the switching frequency.

The connection of the auxiliary circuit slightly increases the average current through L_1 and L_2, which consequently increases the voltage ratio. However, this increase is not considered to design the clamping circuit. Fig. 6 shows the voltage ratio curves of the proposed ACCFHB, the ACCFHB presented in [28] and the conventional CFHB. Therefore, to reach the same voltage ratio of these converters, a lower value of D is used in the proposed ACCFHB.

B. Design Considerations for the Auxiliary Circuit

The resonance between L_{lk} and C_r in the fifth operation mode controls the behavior of the overvoltage across the main switches. Choosing a value for V_{clamp} higher than $V_o/(2n)$, through (14), the following equation is established for C_r

$$C_r = L_{lk}\left(\frac{I_L}{V_{\text{clamp}} - V_o/(2n)}\right)^2. \quad (19)$$

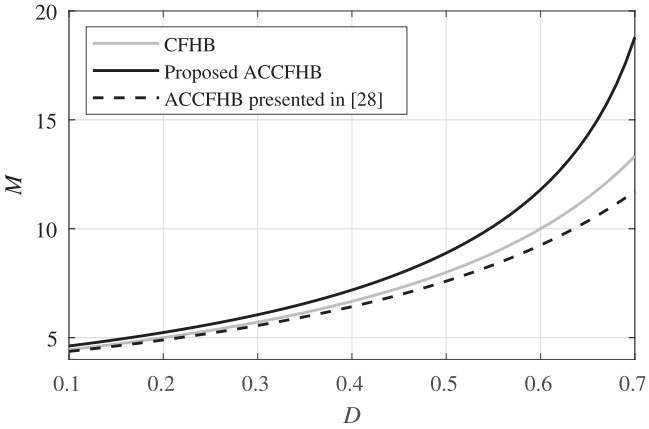

Fig. 6. Voltage ratio curve of the CFHB, the ACCFHB presented in [28], and the proposed ACCFHB.

In addition, to reduce the switching losses in the main switches, the current needs to be reduced to zero at turn-OFF to achieve ZCS condition. Therefore, the current through L_r at the end of stage 1 is designed to be equal to the sum of the currents through L_1 and L_2. Through (3) and (4), the following equation is defined

$$L_r = C_r \frac{V_{\text{clamp}}(V_{\text{clamp}} - 2V_{\text{in}})}{4{I_L}^2}. \quad (20)$$

C. Analysis of Voltage and Current Stress Across the Semiconductors

The main switches are chosen to withstand a maximum voltage equal to V_{clamp}, which is calculated by (14). When the transformer is energized, one of the main switches conducts the current of L_1 and L_2. Therefore, the peak current through these semiconductors is $I_{S_1\text{max}} = I_{S_2\text{max}} = 2I_L$.

The rectifier diodes have to block a voltage level equal to V_o and a maximum current $I_{D_1\text{max}} = I_L/n$.

Regarding the auxiliary circuit, the switch has to withstand a peak current equal to

$$I_{S_a\text{max}} = \frac{V_{\text{clamp}} - V_{\text{in}}}{Z_1} \quad (21)$$

and the maximum voltage across this semiconductor is $V_{S_a\text{max}} = V_{\text{clamp}} - V_{\text{in}}$.

The peak voltage that the auxiliary diodes have to block is equal to V_{clamp}, and the maximum current through these semiconductors is equal to I_L.

D. Comparison of Conventional ACCFHB Converters and the Proposed ACCFHB

Table I shows a comparison of four different ACCFHB in terms of the number of components and driver circuits, voltage stress, and soft-switching features. It is possible to notice that compared to the ACCFHB proposed in [25], [28], and [31], the proposed converter has less active semiconductors, which simplify the driving circuit. Related to these clamping circuits, the main switches of the proposed ACCFHB undergo a higher

TABLE I
COMPARISON OF CONVENTIONAL ACCFHB CONVERTERS AND THE PROPOSED ACCFHB CONVERTER

		[25]	[28]	[31]	Proposed ACCFHB
Number of components	Switches	4	4	4	3
	Diodes	4	4	2	4
	Capacitors	2	2	3	3
	Inductors	2	2	2	3
Soft-switching features	Main switches	ZVS turn-on	ZVS turn-on	-	ZCS turn-off
	Rectifier diodes	-	-	ZCS turn-off	ZCS turn-on and turn-off
	Auxiliary switches	ZVS turn-on	ZVS turn-on	ZVS turn-on	ZCS turn-on and turn-off
Driver circuits	Isolated	2	2	2	1
	Non-isolated	2	2	2	2
Voltage Stress	Main Switches	$V_{in}\frac{D}{1-D}$	$\frac{V_{in}}{1-D}$	$\frac{V_o}{2n}$	$\frac{V_o}{2n}+\sqrt{\frac{L_{lk}}{C_r}}I_L$
	Auxiliary switches	$V_{in}\frac{D}{1-D}$	$\frac{V_{in}}{1-D}$	$\frac{V_o}{2n}$	$\frac{V_o}{2n}-V_{in}+\sqrt{\frac{L_{lk}}{C_r}}I_L$

TABLE II
EXPERIMENTAL PARAMETERS OF THE IMPLEMENTED CONVERTER

Parameter / Component	Value / Details
V_{in}	37 V
V_o	400 V
P_o	300 W
f_s	100 kHz
f_{sa}	200 kHz
Transformer	Transformer ratio: 2.2 Prim: 8 turns, 13 wires #26 AWG Sec: 18 turns, 6 wires #26 AWG Core: EE30/15/14 Thornton L_{lk} = 600 nH
C_1, C_2	470 nF (Polyester 630 V)
L_1, L_2	135 μH 20 turns, 8 wires #26 AWG Core: EE30/15/14 Thornton
C_r	33 nF (Polyester 250 V)
L_r	1.5 μH SMD inductor Würth Elektronik pn:7443320150
S_1, S_2, S_a	IPP110N20N3
D_1, D_2, D_{a1}, D_{a2}	APT10SCD65K

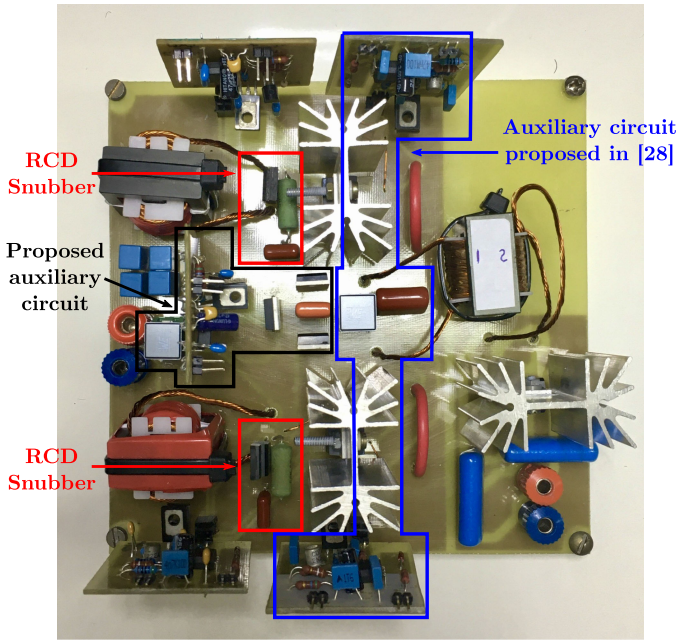

Fig. 7. Experimental prototype (148 mm × 136 mm).

voltage peak, however, the voltage across the auxiliary switch in comparison to [28] and [31] is lower. Unlike these two ACCFHB, the proposed converter achieves ZCS soft-switching not only for the main switches but also for the rectifier diodes. Moreover, the auxiliary switch and diodes also operates under ZCS condition.

IV. EXPERIMENTAL RESULTS

To verify the performance of the proposed converter for a microinverter application, a 300-W prototype was built. The parameters and detailed components of the proposed converter are summarized in Table II, and the experimental prototype is presented in Fig. 7.

Through the inclusion of the auxiliary circuits for voltage clamping, active switches with lower breakdown voltage were used to build the prototype. These semiconductors could not be employed in the conventional CFHB without any clamping circuit, since the main switches undergo high voltage spikes caused by the energy stored in the leakage inductance. The switches selected for the prototype were IPP110N20N3 (200 V, 88 A) from Infineon Technologies, which presents a low on-resistance and gate charge, becoming a suitable semiconductor for HF applications. As diodes, Silicon carbide Schottky APT10SCD65 K (650 V, 10 A) from Microsemi was used, which features low forward voltage and ultralow reverse recovery time and charge. A duty cycle equals 0.567 was used in the proposed ACCFHB for the design operating point.

In Fig. 8, the delay time of half a switching cycle between the commands of the main switches can be verified by the waveforms of the currents through L_1 and L_2. This figure also shows the output voltage at nominal power.

The waveforms of the voltage and current through main switch S_1 and rectifier diode D_1 are presented in Fig. 9. From this figure, it is possible to verify the voltage clamping in

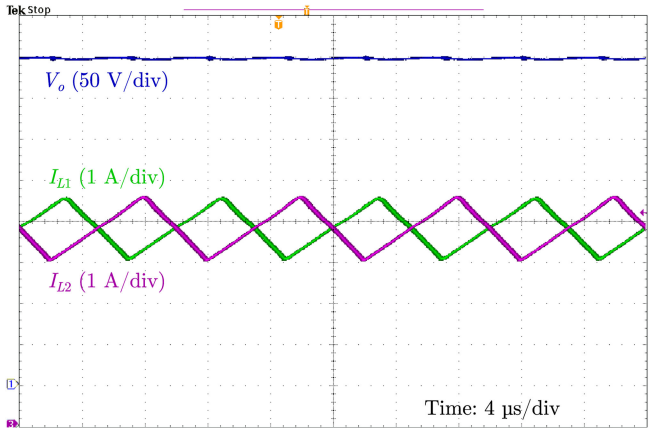

Fig. 8. Current through L_1 and L_2 and output voltage.

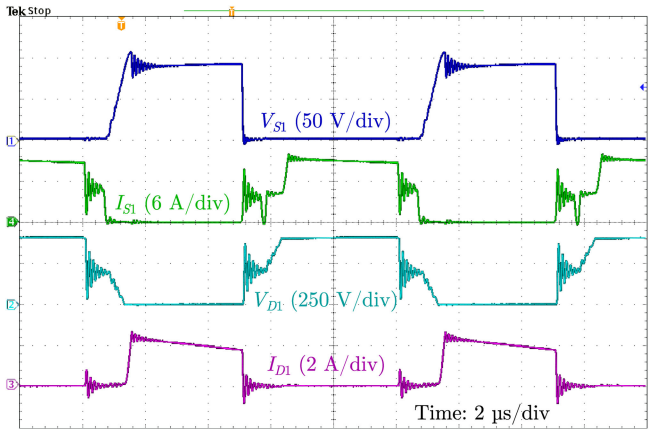

Fig. 9. Current and voltages in S_1 and D_1.

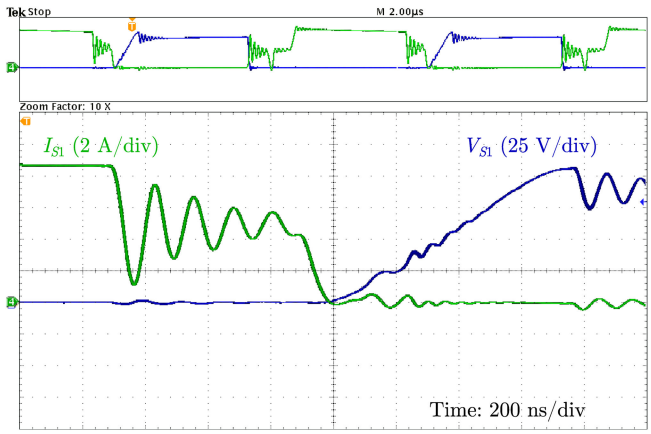

Fig. 10. Detailed ZCS at turn-OFF for S_1.

this switch. Due to the presence of the auxiliary circuit, ZCS condition is achieved for S_1 at turn-OFF, and D_1 turns ON under ZCS. Thus, switching losses and stress in these semiconductors are reduced. An expanded view of these waveforms is shown in Figs. 10 and 11. The oscillations observed in the waveforms are caused mainly by a resonance occurring between

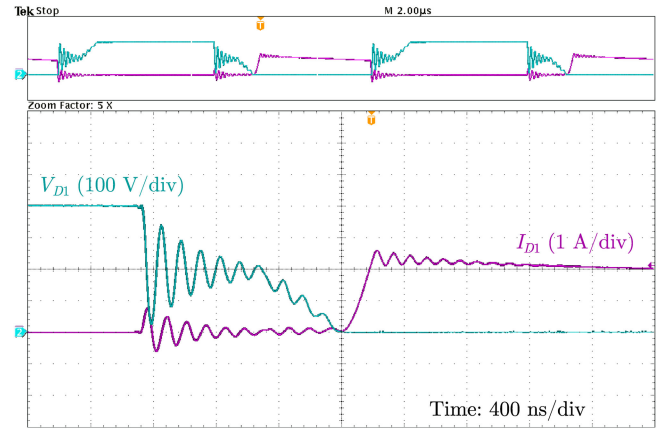

Fig. 11. Detailed ZCS at turn-ON for D_1.

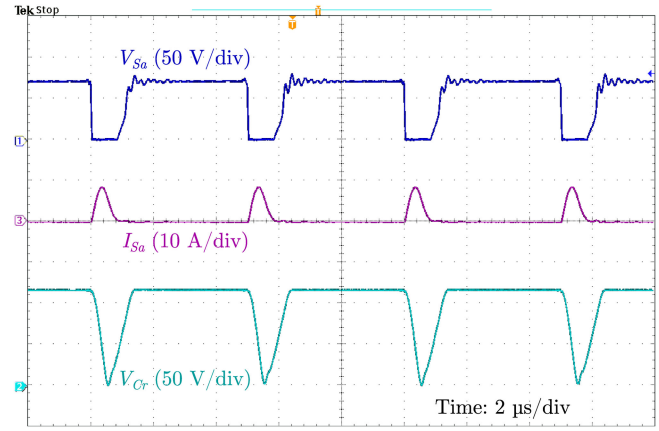

Fig. 12. Voltage and current in S_a and voltage across C_r.

the leakage capacitance of the rectifier diodes and the leakage inductance of the transformer when both diodes are not conducting. To minimize the amplitude of these oscillations and thereby reduce the losses from this effect, diodes that feature low junction capacitance can be used in the rectifier stage.

The waveforms of the auxiliary switch and clamping capacitor are presented in Fig. 12. From this figure, it is possible to verify that the voltage across S_a is also clamped. Besides, Fig. 13 shows in more detail the ZCS condition at turn-OFF being achieved for the auxiliary switch, as well as a commutation near ZCS obtained at turn-ON, due to the resonance established in operation mode 1.

The converter was also tested for an input voltage range from 34 to 40 V to check the performance at different operating points. Fig. 14 presents the measured efficiency of the proposed converter for various load conditions using the Yokogawaga WT1800 high-performance power analyzer. The proposed converter, reached a value equals 95.6% at full load. Peak efficiency of 96.2% was obtained for 40 V input voltage, and a minimum value of 89.2% was reached for 34 V input voltage.

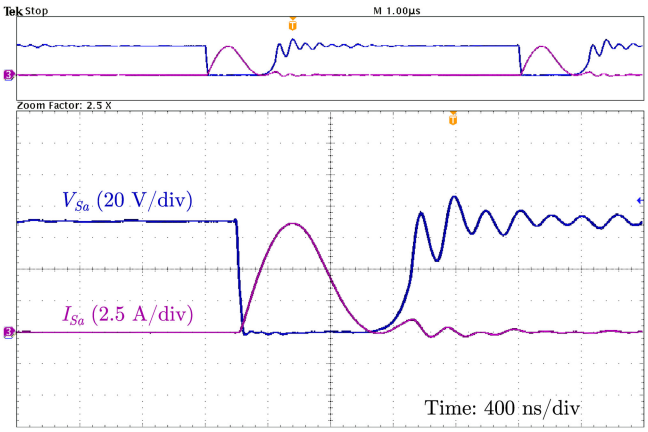

Fig. 13. Detailed ZCS for S_a.

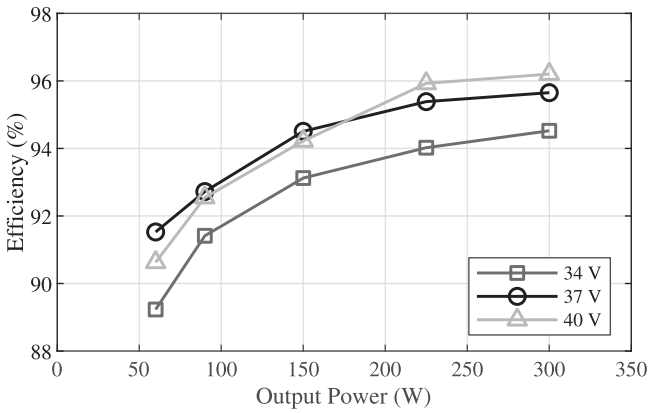

Fig. 14. Measured efficiency of the proposed converter for various load and input voltage conditions.

V. Power Losses Analysis

To obtain an efficiency improvement for the CFHB through the connection of the auxiliary circuit, the power losses in the clamping circuit must be smaller than the energy savings from the soft-switching achievements. Since the main switches of the CFHB undergo high overvoltages without any clamping circuit, an RCD snubber was designed based on [32] and connected to each switch of the conventional CFHB. The same printed circuit board (PCB) of the CFHB without the proposed clamping circuit was used, as can be observed in Fig. 7. The diodes employed in the RCD snubbers were 15ETH06 (600 V, 15 A) from International Rectifier. Snubber resistors $R_s = 82\ \Omega$ and capacitors $C_s = 10$ nF were used. Considering the parameters specified in Table II, a duty cycle equals 0.611 was applied to each main switch.

Also, the clamping circuit presented in Fig. 1 was connected to the same PCB of the CFHB presented in Fig. 7 to compare the efficiency results. For the auxiliary switches S_{a_1} and S_{a_2}, IPP320N20N3 (200 V, 34 A) from Infineon Technologies were used, since this model features lower gate charge and the current through these semiconductors is lower compared to the main switches. A clamping capacitor $C_{\text{clamp}} = 1\ \mu$F and a series inductor $L_s = 4.7\ \mu$F were used. A duty cycle equal to 0.626 was applied to each main switch for the ACCFHB with the clamping circuit presented in Fig. 1, since it features a lower voltage ratio.

TABLE III
Individual Power Loss Breakdown Employing Each Clamping Circuit

Component	Loss	RCD (W)	Proposed (W)	[28] (W)
S_1=S_2	Conduction	0.336	0.324	0.372
	Switching	3.595	2.214	1.577
	Total	3.931	2.538	1.949
D_1=D_2	Conduction	1.072	1.072	1.37
	Switching	0.9	ZCS	0.9
	Total	1.972	1.072	2.27
S_a	Conduction	-	0.089	-
	Switching	-	ZCS	-
	Total	-	0.089	-
D_{a1}=D_{a2}	Conduction	-	0.934	-
	Switching	-	0.204	-
	Total	-	1.138	-
L_r	Total	-	0.029	-
C_r	Total	-	0.584	-
L_1=L_2	Total	0.63	0.806	0.63
Transformer	Total	1.971	1.983	2.203
RCD	Total	3.078	-	-
S_{a1}=S_{a2}	Conduction	-	-	0.047
	Switching	-	-	1.678
	Total	-	-	1.725
L_s	Total	-	-	0.144
C_{clamp}	Total	-	-	0.099

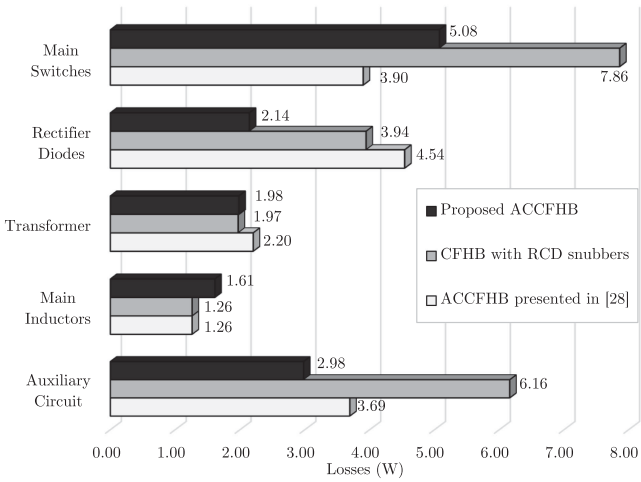

Fig. 15. Calculated total losses for the CFHB employing each clamping circuit considering an input voltage equals 37 V and an output voltage equal to 400 V at full load.

An individual power loss breakdown based on [33] for each component is shown in Table III, while Fig. 15 gives the total losses of the CFHB employing each clamping circuit, both at full load. The losses in the auxiliary circuits include those in the resonant and series inductors, and the clamping capacitor, as well as the losses in the auxiliary switches and diodes. In the same way, the losses in the RCD snubbers represent those in the capacitors, in the resistors, and in the snubber diodes.

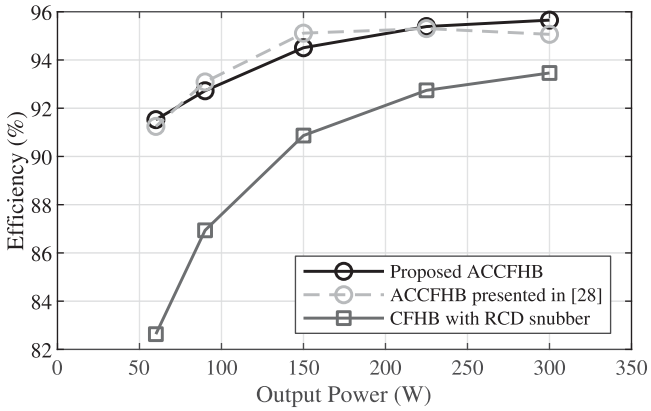

Fig. 16. Measured efficiency of the CFHB with each clamping circuit for various load conditions at $V_{\text{in}} = 37$ V and $V_o = 400$ V.

Also, this figure presents the losses in the transformer, inductors, main switches, and rectifier diodes for each case.

Through the power loss calculation, it is possible to verify significant savings in the main switches for both ACCFHB compared to the CFHB employing RCD snubbers. A loss reduction of about 35% was obtained for the main switches of the proposed ACCFHB. Also, through ZCS in the rectifier diodes, a power loss saving equal to 45% was achieved through the proposed auxiliary circuit. The ACCFHB proposed in [28] presented more losses in the transformer, since the peak and rms current through this element is higher. Moreover, its auxiliary circuit presents slightly more power losses than the proposed clamping circuit, which are mainly concentrated in conduction and reverse recovery losses of the body diode of S_{a1} and S_{a2} at ZVS turn-ON. The losses in the auxiliary diodes represented 76% of the total losses in the proposed clamping circuit. Compared to the CFHB with RCD snubbers, an efficiency increase of 2.2% was obtained for the proposed ACCFHB at full load.

The efficiency of the three clamping circuits connected individually to the CFHB was measured using the Yokogawa WT1800. Fig. 16 presents results for $V_{\text{in}} = 37$ V and $V_o = 400$ V employing each clamping circuit for the CFHB converter. The peak efficiency for the CFHB with RCD snubber was 93.4% at full load, while the ACCFHB presented in [28] achieved 95.3% at 50% load and the proposed converter reached 95.6% at full load.

VI. Conclusion

In this article, an auxiliary circuit for the CFHB converter was proposed to overcome the usual high-voltage spikes in this topology. In addition to clamping the overvoltages across the main switches, the auxiliary circuit provides ZCS condition to the main switches at turn-OFF and to the rectifier diodes at both turn-ON and turn-OFF, reducing significantly the switching losses and stress in these components.

With the proposed clamping circuit, the voltage ratio of the conventional CFHB increases, reducing the duty cycle value. Moreover, the auxiliary switch operates under ZCS condition and the voltage in this semiconductor is also clamped. Due to the clamping action, it is possible to select semiconductors with lower breakdown voltage for the converter, which generally feature lower on-resistance and contribute to improving efficiency.

Also, in the same PCB of the proposed converter, connections for RCD snubbers and the active clamping circuit presented in [28] were included to perform a comparative analysis of losses. Compared to the CFHB with RCD snubbers, the proposed converter obtained an efficiency increase of 2.2% at full load.

Compared to other clamping circuits presented in the literature for the CFHB, the proposed auxiliary circuit employs only one active switch, reducing the number of drivers and auxiliary sources. Unlike some designs of ACCFHB converters, the proposed one does not demand a series inductor with the transformer.

References

[1] M. Kim and S. Choi, "A fully soft-switched single switch isolated dc–dc converter," *IEEE Trans. Power Electron.*, vol. 30, no. 9, pp. 4883–4890, Sep. 2015.

[2] P. U R and A. K. Rathore, "Extended range ZVS active-clamped current-fed full-bridge isolated dc/dc converter for fuel cell applications: Analysis, design, and experimental results," *IEEE Trans. Ind. Electron.*, vol. 60, no. 7, pp. 2661–2672, Jul. 2013.

[3] J. Roy, Y. Xia, and R. Ayyanar, "High step-up transformerless inverter for ac module applications with active power decoupling," *IEEE Trans. Ind. Electron.*, vol. 66, no. 5, pp. 3891–3901, May 2019.

[4] K. R. Sree, A. K. Rathore, E. Breaz, and F. Gao, "Soft-switching non-isolated current-fed inverter for pv/fuel cell applications," *IEEE Trans. Ind. Appl.*, vol. 52, no. 1, pp. 351–359, Jan. 2016.

[5] W. Li, J. Liu, J. Wu, and X. He, "Design and analysis of isolated ZVT boost converters for high-efficiency and high-step-up applications," *IEEE Trans. Power Electron.*, vol. 22, no. 6, pp. 2363–2374, Nov. 2007.

[6] F. L. Tofoli, D. de C. Pereira, W. Josias de Paula, and D. de S. Oliveira Jnior, "Survey on non-isolated high-voltage step-up dc–dc topologies based on the boost converter," *IET Power Electron.*, vol. 8, no. 10, pp. 2044–2057, 2015.

[7] M. Fekri, N. Molavi, E. Adib, and H. Farzanehfard, "High voltage gain interleaved dc–dc converter with minimum current ripple," *IET Power Electron.*, vol. 10, no. 14, pp. 1924–1931, 2017.

[8] W. Li and X. He, "Review of nonisolated high-step-up dc/dc converters in photovoltaic grid-connected applications," *IEEE Trans. Power Electron.*, vol. 58, no. 4, pp. 1239–1250, Apr. 2011.

[9] M. Forouzesh, Y. Shen, K. Yari, Y. P. Siwakoti, and F. Blaabjerg, "High-efficiency high step-up dc–dc converter with dual coupled inductors for grid-connected photovoltaic systems," *IEEE Trans. Power Electron.*, vol. 33, no. 7, pp. 5967–5982, Jul. 2018.

[10] L. Zhu, "A novel soft-commutating isolated boost full-bridge ZVS-PWM dc–dc converter for bidirectional high power applications," *IEEE Trans. Power Electron.*, vol. 21, no. 2, pp. 422–429, Mar. 2006.

[11] M. Muhammad, M. Armstrong, and M. A. Elgendy, "A nonisolated interleaved boost converter for high-voltage gain applications," *IEEE J. Emerg. Sel. Topics Power Electron.*, vol. 4, no. 2, pp. 352–362, Jun. 2016.

[12] A. M. S. S. Andrade, L. Schuch, and M. L. da Silva Martins, "Analysis and design of high-efficiency hybrid high step-up dc–dc converter for distributed PV generation systems," *IEEE Trans. Ind. Electron.*, vol. 66, no. 5, pp. 3860–3868, May 2019.

[13] M. Forouzesh, Y. P. Siwakoti, S. A. Gorji, F. Blaabjerg, and B. Lehman, "Step-up dc–dc converters: A comprehensive review of voltage-boosting techniques, topologies, and applications," *IEEE Trans. Power Electron.*, vol. 32, no. 12, pp. 9143–9178, Dec. 2017.

[14] X. Kong and A. M. Khambadkone, "Analysis and implementation of a high efficiency, interleaved current-fed full bridge converter for fuel cell system," *IEEE Trans. Power Electron.*, vol. 22, no. 2, pp. 543–550, Mar. 2007.

[15] H. Kim, C. Yoon, and S. Choi, "An improved current-fed zvs isolated boost converter for fuel cell applications," *IEEE Trans. Power Electron.*, vol. 25, no. 9, pp. 2357–2364, Sep. 2010.

[16] U. R. Prasanna, A. K. Rathore, and S. K. Mazumder, "Novel zero-current-switching current-fed half-bridge isolated dc/dc converter for fuel-cell-based applications," *IEEE Trans. Ind. Appl.*, vol. 49, no. 4, pp. 1658–1668, Jul. 2013.
[17] P. Xuewei and A. K. Rathore, "Current-fed soft-switching pushpull front-end converter-based bidirectional inverter for residential photovoltaic power system," *IEEE Trans. Power Electron.*, vol. 29, no. 11, pp. 6041–6051, Nov. 2014.
[18] and, J. Abu-Qahouq, and I. Batarseh, "Active-clamp snubbers for isolated half-bridge dc-dc converters," *IEEE Trans. Power Electron.*, vol. 20, no. 6, pp. 1294–1302, Nov. 2005.
[19] Q. Wu, Q. Wang, J. Xu, and Z. Xu, "Active-clamped ZVS current-fed push–pull isolated dc/dc converter for renewable energy conversion applications," *IET Power Electron.*, vol. 11, no. 2, pp. 373–381, 2018.
[20] M. Das and V. Agarwal, "Design and analysis of a high-efficiency dc–dc converter with soft switching capability for renewable energy applications requiring high voltage gain," *IEEE Trans. Ind. Electron.*, vol. 63, no. 5, pp. 2936–2944, May 2016.
[21] C. Vartak, A. Abramovitz, and K. Ma Smedley, "Analysis and design of energy regenerative snubber for transformer isolated converters," *IEEE Trans. Power Electron.*, vol. 29, no. 11, pp. 6030–6040, Nov. 2014.
[22] V. R. Vakacharla and A. K. Rathore, "Current-fed isolated lcc-t resonant converter with zcs and improved transformer utilization," *IEEE Trans. Ind. Electron.*, vol. 66, no. 4, pp. 2735–2745, Apr. 2019.
[23] S. Salehi Dobakhshari, J. Milimonfared, M. Taheri, and H. Moradisizkoohi, "A quasi-resonant current-fed converter with minimum switching losses," *IEEE Trans. Power Electron.*, vol. 32, no. 1, pp. 353–362, Jan. 2017.
[24] F. Xue, R. Yu, and A. Q. Huang, "A 98.3% efficient gan isolated bidirectional dc–dc converter for dc microgrid energy storage system applications," *IEEE Trans. Ind. Electron.*, vol. 64, no. 11, pp. 9094–9103, Nov. 2017.
[25] S.-K. Han, H.-K. Yoon, G.-W. Moon, M.-J. Youn, Y.-H. Kim, and K.-H. Lee, "A new active clamping zero-voltage switching PWM current-fed half-bridge converter," *IEEE Trans. Power Electron.*, vol. 20, no. 6, pp. 1271–1279, Nov. 2005.
[26] A. Rathore, A. K. S. Bhat, and R. Oruganti, "Analysis and design of active clamped zvs current-fed dc-dc converter for fuel-cell to utility-interface application," in *Proc. IEEE Int. Conf. Ind. Inf. Syst.*, Aug. 2007, pp. 503–508.
[27] A. K. Rathore, A. K. S. Bhat, and R. Oruganti, "Wide range zvs active-clamped l-l type current-fed dc-dc converter for fuel cells to utility interface: Analysis, design and experimental results," in *Proc. IEEE Energy Convers. Congr. Expo.*, Sep. 2009, pp. 1153–1160.
[28] S. Jang, C. Won, B. Lee, and J. Hur, "Fuel cell generation system with a new active clamping current-fed half-bridge converter," *IEEE Trans. Energy Convers.*, vol. 22, no. 2, pp. 332–340, Jun. 2007.
[29] S. A. Teston, E. G. Carati, J. P. da Costa, R. Cardoso, and C. M. de O. Stein, "Comparison of two connection possibilities of the clamp capacitor in the active-clamped zvs current-fed half-bridge converter," in *Proc. IEEE 13th Brazilian Power Electron. Conf. 1st Southern Power Electron. Conf.*, Nov. 2015, pp. 1–6.
[30] H. Bahrami, E. Adib, S. Farhangi, H. Iman-Eini, and R. Golmohammadi, "Zcs-pwm interleaved boost converter using resonance-clamp auxiliary circuit," *IET Power Electron.*, vol. 10, no. 3, pp. 405–412, 2017.
[31] J. Kwon and B. Kwon, "High step-up active-clamp converter with input-current doubler and output-voltage doubler for fuel cell power systems," *IEEE Trans. Power Electron.*, vol. 24, no. 1, pp. 108–115, Jan. 2009.
[32] N. Mohan, T. M. Undeland, and W. P. Robbins, *Power Electronics - Converters, Applications and Design*, 2nd ed. New York, NY, USA: Wiley, 1995.
[33] D. Graovac, M. Purschel, and A. Kiep, "MOSFET power losses calculation using the data-sheet parameters," Infineon Technologies AG, Neubiberg, Germany, Jul. 2006.

Cassiano Ferro Moraes received the B.S. degree in electrical engineering from the Federal University of Technology—Paraná, Pato Branco, Brazil, in 2017, where he is currently working toward the M.S. degree.

His research interests include high-frequency converters for distributed generation, isolated dc–dc converters, and soft-switching techniques.

Emerson Giovani Carati received the graduate, master's, and the Ph.D. degrees in electrical engineering from the Federal University of Santa Maria, Santa Maria, Brazil, in 1996, 1999, and 2003, respectively.

Since 2003, he has been a Professor with the Federal University of Technology—Paraná, Pato Branco, Brazil, where he is currently a Permanent Faculty of the Graduate Program in electrical engineering. His research interests include digital control and digital signal processing, with applications in electrical machines drives, distributed power generation, and static converters systems.

Jean Patric da Costa was born in Santa Maria, Brazil, in 1979. He received the B.S. degree in electrical engineering from the Federal University of Santa Maria (UFSM), Santa Maria, Brazil, in 2004, and the master's and Ph.D. degrees from the UFSM, in 2006, and 2010, respectively.

He is currently a Professor with the Department of Electrical Engineering, Federal University of Technology—Paraná, Pato Branco, Brazil. His research interests include control of static converters, smart grids, ancillary services, and distribution networks with distributed generators.

Rafael Cardoso received the B.S. degree in electrical engineering from the Federal University of Santa Maria (UFSM), Santa Maria, Brazil, in 2001, the M.Sc. degree in electronic and computer science from the Technological Institute of Aeronautics, São Paulo, Brazil, in 2003, and the Ph.D. degree in electrical engineering from the UFSM, in 2008.

Since 2006, he has been with the Federal University of Technology—Paraná, Pato Branco, Brazil, where he is currently a Professor. His research interests include control systems applications, signal processing, active power filtering, and the control of static converters for smart-grids and power quality.

Carlos Marcelo de Oliveira Stein was born in Santiago, Brazil, in 1970. He received the B.S., M.S., and Ph.D. degrees in electrical engineering from the Federal University of Santa Maria, Santa Maria, Brazil, in 1996, 1997, and 2003, respectively.

Since 2003, he has been with the Federal University of Technology—Paraná, Pato Branco, Brazil, where he is currently a Professor. His research interests include high-frequency power converter topologies, distributed generation, power supplies, and soft-switching techniques.